SNUTP 97-050

Preroughening transitions in a model for Si and Ge (001) type crystal surfaces

Jae Dong Noh

Center for Theoretical Physics, Seoul National University, Seoul 151-742, Korea

Marcel den Nijs

Department of Physics, University of Washington, Seattle, WA 98195, USA

(February 7, 2008)

Abstract

The uniaxial structure of Si and Ge (001) facets leads to nontrivial topological properties of steps and hence to interesting equilibrium phase transitions. The disordered flat phase and the preroughening transition can be stabilized without the need for step-step interactions. A model describing this is studied numerically by transfer matrix type finite-size-scaling of interface free energies. Its phase diagram contains a flat, rough, and disordered flat phase, separated by roughening and preroughening transition lines. Our estimate for the location of the multicritical point where the preroughening line merges with the roughening line, predicts that Si and Ge (001) undergo preroughening induced simultaneous deconstruction transitions.

I. INTRODUCTION

The structure of the (001) facets of Si and Ge is very interesting from the point of view of equilibrium phase transitions. These surfaces have an uniaxial reconstruction [1], where the uniaxial direction switches by 90° at alternating surface heights. Due to this, the mono-atomic and bi-atomic steps have nontrivial topological properties. This atomic structure and the crossover from mono-atomic steps in non-vicinal surfaces to bi-atomic steps in vicinal surfaces have been studied extensively [2–5]. Roughening type phase transitions in these surfaces close to the melting temperature, are an another interesting topic [6,7]. One of us suggested earlier [7] that this unusual topology leads to disordered flat (DOF) phases and preroughening (PR) transitions without a need for step-step interactions. In this paper we present a detailed numerical transfer matrix finite-size-scaling (FSS) study of the model introduced in Ref. [7].

Consider a surface like Si (001), but one which does not reconstruct. Such a surface is still uniaxial and it still switches by 90° at alternating surface heights. At finite temperature T, thermodynamically-excited steps appear. They separate domains of flat regions. The uniaxial structure leads to two distinct types of mono-atomic steps, labeled by S_A and S_B. The subscripts denote whether the uniaxial direction in the upper terrace near the step is parallel (A) or normal (B) to the step edge. Considering the fact that the uniaxial direction switches by 90° at alternating surface heights, one finds, as shown in Fig. 1, that the steps have the following topological properties [7]: (i) If two neighboring parallel steps are of the same type, one must be an up-step and the other a down-step. (ii) If a step turns over 90° it must change its type, from S_A to S_B and vice versa. Bi-atomic steps exist as well [5], but they are probably free-energetically unfavorable close to the roughening temperature [7].

These topological properties imply that terrace excitations have an ellipsoid shape, and that the long axes of nested terraces are parallel (perpendicular) if the height change is up-down or down-up (up-up or down-down) across the nested terraces. This creates an entropic penalty against forming hills and valleys. In other words, it opens the possibility

to stabilize a DOF phase without the need for step-step interactions [7]. Thus far step-step interactions were believed to be crucial for the existence of DOF phases. In this surface topology, however, the DOF phase originates directly from the uniaxial structure of the surface.

The restricted solid-on-solid (RSOS) model on a square lattice with the Hamiltonian

$$\mathcal{H} = \sum_{\mathbf{r}} \left\{ K(h(x+1,y) - h(x,y))^2 + \Delta \sin\left[\frac{\pi}{2}(h(x,y) + h(x+1,y))\right] \right\} + \sum_{\mathbf{r}} \left\{ K(h(x,y+1) - h(x,y))^2 - \Delta \sin\left[\frac{\pi}{2}(h(x,y) + h(x,y+1))\right] \right\} , \quad (1)$$

was introduced in Ref. [7] to describe the thermodynamic properties of such steps in more detail. $h(\mathbf{r})$ is an integer-valued height variable at each site $\mathbf{r} = (x, y)$. Height differences between the nearest neighbor sites are restricted to 0 and ± 1. This means that only mono-atomic steps are allowed. Bi-atomic steps can be included in a later stage if experimental evidence shows they remain important close to roughening temperatures. The model of Eq. (1) contains two parameters. The Δ terms distinguish between S_A and S_B-type steps: $E_A = K - \Delta$ and $E_B = K + \Delta$ are the step energies. Without loss of generality, the uniaxial direction is taken to run vertically (horizontally) at even (odd) heights.

The model Hamiltonian contains two limiting cases. The conventional RSOS model at $\Delta = 0$ displays a Kosterlitz-Thouless (KT) type roughening transition between the flat and rough phases [8]. On the other hand, in the limit where $E_A = 0$ and $T = 0$, S_A steps cost no energy while S_B steps are frozen out. In a typical configuration the surface contains a set of randomly-placed parallel S_A steps in the form of straight lines. However, the topological rule (i) requires that they are alternating up and down steps. This is a typical morphology of surfaces in the DOF phase [9]. The DOF phase is an intermediate phase between the flat and rough phases, where the steps are disordered positionally but have long-range up-down-up-down order. It was argued in Ref. [7] that this DOF type structure is stable at finite temperatures, in terms of a Fermionic type perturbation theory.

In this paper, we investigate the phase diagram quantitatively through a detailed transfer matrix FSS study. It is important to confirm the existence of the DOF phase numerically.

The analysis in Ref. [7] was mostly qualitative. The other purpose of this work is to obtain a good estimate for the critical value of the ratio $r \equiv E_B/E_A$, below which the DOF phase disappears, see Fig. 2. In real surfaces this ratio takes specific values. For example, observations of step fluctuations in STM and LEED experiments yield for Si (001) that $r \sim 3$ ($E_A = 325K$ and $E_B = 1045K$) [10]. By comparing this ratio with the critical value r_c, one can decide which path the Si (001) surface follows.

Our model, Eq. (1), does not incorporate the 2×1 type dimerized surface reconstruction of Si and Ge (001). Therefore it does not describe the competition between surface reconstruction and surface roughening in those surfaces. This issue was addressed in Ref. [7]. The preroughening line in Fig. 2 is most likely replaced by a PR induced simultaneous deconstruction transition and the roughening line segment at $r < r_c$ by a roughening induced simultaneous deconstruction transition. A proper quantitative description of this requires at least a RSOS model coupled to an Ising model. We did not study such a model, since the number of degrees of freedom becomes too large to obtain meaningful transfer matrix FSS results. The precise location of r_c in Fig. 2 is the result of a delicate entropy balancing act of nested terraces associated with the peculiar 90° switching in the uniaxial direction. Our value of r_c should be meaningful for Si and Ge (001) if the coupling with the Ising degrees of freedom does not change the value of r_c by too much, which is a reasonable assumption.

In Sec. II, we introduce various kinds of interface free energies. They decompose into the free energies of S_A and S_B type steps, and show distinct FSS behaviors in the flat, DOF, and rough phases. We obtain the phase diagram Fig. 2, by evaluating these interface free energies using the transfer matrix method. The numerical results and a summary are presented in Sec. III.

II. INTERFACES AND THE TRANSFER MATRIX FORMALISM

Consider the model given by Eq. (1) on a finite $N \times M$ lattice with periodic boundary conditions (PBC's), $h(x+N, y) = h(x, y)$ and $h(x, y+M) = h(x, y)$. The ordered flat phase

is commensurate with PBC's. Other (gauge invariant) boundary conditions (BC's) create frustrations, and thus impose steps in the surface. The interface free energy η is defined as the excess free energy per unit length for each type of BC compared to that of PBC's. Their FSS behaviors are different in the various phases. We obtain the structure of the phase transitions by studying suitable ones.

The Hamiltonian in Eq. (1) is invariant under the global transformations

$$h(\mathbf{r}) \to h(\mathbf{r}) + 2n \tag{2}$$

$$h(\mathbf{r}) \to -h(\mathbf{r}) + 1 \ (\text{mod } 2) \ , \tag{3}$$

for all integers n. So it is natural to consider the following boundary conditions: step type BC's with $h(x+N, y) = h(x, y) + 2$ and $h(x, y+M) = h(x, y)$; and anti-periodic type BC's with $h(x+N, y) = -h(x, y) + 1 \ (\text{mod } 2)$ and $h(x, y+M) = h(x, y)$. We will refer to them as H1 and H2 respectively. Similarly, V1 and V2 refer to the same BC's but with the roles of the M and N interchanged. The interface free energies are defined by

$$\eta_\alpha = -\frac{1}{M} \ln \frac{Z_\alpha}{Z_{PBC}} \ , \ (\alpha = \text{H1}, \ \text{H2})$$
$$\eta_\beta = -\frac{1}{N} \ln \frac{Z_\beta}{Z_{PBC}} \ , \ (\beta = \text{V1}, \ \text{V2}) \ .$$

with Z_α the partition function satisfying the boundary condition α, and all energies and free energies measured in units of $k_B T$.

Figure 3 shows the topological frustrations induced by these BC's. H1 and V1 require at least two parallel steps; one is an S_A type step and the other an S_B type step (see Figs. 3 (a) and (c)). Therefore, η_{H1} and η_{V1} decompose into $\eta_A + \eta_B$; with η_A and η_B the S_A and S_B step free energies. On the other hand, H2 and V2 can be satisfied by configurations with only one S_A type step (see Figs. 3 (b) and (d)). Therefore, η_{H2} and η_{V2} are equal into η_A.

These interface free energies must behave in a specific way in each type of phase. The step free energy η_B is finite in the flat phase and also in the DOF phase, but vanishes in the rough phase. The step free energy η_A, is finite in the flat phase, but vanishes in both the DOF and rough phase. Therefore, in the flat phase, all four η_α (α=H1, H2, V1, V2) are

finite. In the DOF phase, $\eta_{\rm H1}$ and $\eta_{\rm V1}$ remain finite, but $\eta_{\rm H2}$ and $\eta_{\rm V2}$ vanish (exponentially with system size). In the rough phase, all four η_α vanish (as a powerlaw in the infinite M and/or N limit).

The rough phase is a critical phase where its critical fluctuations are described by the Gaussian model. The height-difference correlation function diverges logarithmically with distance:

$$\langle (h(\mathbf{r}) - h(\mathbf{r}'))^2 \rangle \simeq \frac{1}{\pi K_g} \ln |\mathbf{r} - \mathbf{r}'| \ ,$$

where K_g is the coupling constant of the Gaussian model (also called the stiffness constant). It varies continuously in the rough phase and takes the universal value $\frac{\pi}{2}$ at roughening transitions. The interface free energies vanish in the rough phase as powerlaws. In a semi-infinite geometry $M \to \infty$, $\eta_{\rm H1}$ and $\eta_{\rm H2}$ scale asymptotically as [9]

$$\eta_{\rm H1} = \frac{2\zeta K_g}{N} \tag{4}$$

$$\eta_{\rm H2} = \frac{\pi\zeta}{4N} \ , \tag{5}$$

where ζ is the aspect ratio of the lattice constants in the spatial and time-like directions.

We evaluate the interface free energies through the transfer matrix. Consider the transfer matrix for a square lattice rotated by 45° as shown in Fig. 4. In our units the aspect ratio is equal to $\zeta = 2$; one unit in time, a_τ is twice as big as the spatial unit a_x. A height configuration $(h_0, h_1, \ldots, h_N)$ in a row is represented by a state vector $|h_0, h_1, \ldots, h_N\rangle$. It is convenient to replace the height variables by step variables $s_i \equiv h_i - h_{i-1}$, with $i = 1, \ldots, N$. They take only the values 0, and ± 1 due to the restricted solid-on-solid condition. The surface configuration in each row is therefore represented by $|h_0, \mathbf{s}\rangle$ where $\mathbf{s}$ stands for $(s_1, s_2, \ldots, s_N)$. The elements of the transfer matrix $\mathbf{T}$ are the Boltzmann weights associated with height configurations $|h_0, \mathbf{s}\rangle$ and $|h_0', \mathbf{t}\rangle$ in successive rows. $\mathbf{T}$ is sparse, and can be expressed in terms of a product over local vertex-type scattering matrices, acting on the $|h_0, \mathbf{s}\rangle$ and $|h_0', \mathbf{t}\rangle$ in successive rows and intermediate internal step variables $\mathbf{u}$, defined in Fig. 4.

In the case of PBC's the step variables satisfy the conditions $s_{i+N} = s_i$ and $\sum_{i=1}^{N} s_i = 0$ in all rows. The partition function, $Z_{\rm PBC} = {\rm Tr}\ \mathbf{T}_{\rm PBC}^M$, and the free energy, are obtained from the largest eigenvalue $e^{-E_{\rm PBC}}$ of $\mathbf{T}_{\rm PBC}$ in the $M \to \infty$ limit.

The transfer matrices $\mathbf{T}_{\rm H1}$ and $\mathbf{T}_{\rm H2}$ for the horizontal BC's H1 and H2 are easily defined. Only the conditions the step variables must satisfy change: In the case of H1, the step variables are again periodic, $s_{i+N} = s_i$, but with $\sum_{i=1}^{N} s_i = 2$ in all rows. In the case of H2, the step variables are anti-periodic, $s_{i+N} = -s_i$, with no restriction in the value of $\sum_{i=1}^{N} s_i$. The partition function in each case is given by $Z_\alpha = {\rm Tr}\ \mathbf{T}_\alpha^M$ and the free energy, in the $M \to \infty$ limit, is again obtained from the largest eigenvalue e^{-E_α} of $\mathbf{T}_\alpha$ (α = H1 and H2). So the interface free energies are given by

$$\eta_{\rm H1} = E_{\rm H1} - E_{\rm PBC} \tag{6}$$

$$\eta_{\rm H2} = E_{\rm H2} - E_{\rm PBC}\ . \tag{7}$$

The transfer matrices for the two vertical BC's are more intricate. They involve the symmetry properties Eq. (2) and Eq. (3) of the transfer matrix with PBC's. The translation invariance in the surface heights, Eq. (2), implies that $\mathbf{T}_{\rm PBC}$ commutes with the symmetry operator

$$\mathbf{P}|h, \mathbf{s}\rangle = |h+2, \mathbf{s}\rangle\ . \tag{8}$$

Therefore, it is useful to distinguish between two classes of surface states, $\{|e, \mathbf{s}\rangle\}$ and $\{|o, \mathbf{s}\rangle\}$, i.e., all states with h even and odd, respectively. From the parity type symmetry property Eq. (3) it follows that $\mathbf{T}_{\rm PBC}$ commutes also with the operator $\mathbf{R}$, defined by

$$\mathbf{R}|e, \mathbf{s}\rangle = |o, -\mathbf{s}\rangle$$

$$\mathbf{R}|o, \mathbf{s}\rangle = |e, -\mathbf{s}\rangle$$

where $-\mathbf{s}$ stands for $(-s_1, -s_2, \ldots, -s_N)$. The transfer matrices for the vertical BC's can be expressed in term of $\mathbf{T}_{\rm PBC}$, $\mathbf{P}$, and $\mathbf{R}$ as $Z_{\rm V1} = {\rm Tr}\ [\mathbf{T}_{\rm PBC}^M \mathbf{P}]$ and $Z_{\rm V2} = {\rm Tr}\ [\mathbf{T}_{\rm PBC}^M \mathbf{R}]$.

To evaluate $Z_{\rm V1}$ one needs to keep track of the height in the first column modulo 4. This makes this boundary condition less useful than its horizontal counter part H1, where we do

not need to keep track of the absolute height of the surface, and therefore can drop the h_0 label of the surface configurations altogether. So we discard $Z_{\rm V1}$ in the following analysis.

On the other hand, $Z_{\rm V2}$ is very useful. It can be written as

$$Z_{\rm V2} = \sum_i e^{-ME_{\rm PBC}(i)} - \sum_i e^{-ME'_{\rm PBC}(i)} \ , \tag{9}$$

where $e^{-E_{\rm PBC}(i)}$ ($e^{-E'_{\rm PBC}(i)}$) is the ith largest eigenvalue of $\mathbf{T}_{\rm PBC}$ in the $R=+1$ (-1) sector. By the $R=+1$ (-1) sector, we mean the set of state vectors which are eigenvectors of $\mathbf{R}$ with the eigenvalue $+1$ (-1). Unlike horizontal boundary conditions, $\eta_{\rm V2}$ depends on the entire eigenvalue spectra. However, in the thermodynamic limit, it can be approximated, up to the leading order, as

$$\eta_{\rm V2} \simeq -\frac{1}{N} \ln \frac{e^{-ME_{\rm PBC}} - e^{-ME'_{\rm PBC}}}{e^{-ME_{\rm PBC}} + e^{-ME'_{\rm PBC}}} \ ,$$

where $E_{\rm PBC}$ ($E'_{\rm PBC}$) is the largest eigenvalue of $\mathbf{T}_{\rm PBC}$ in the $R=+1$ (-1) sector. So the scaling behavior of $\eta_{\rm V2}$ is determined from the quantity

$$m = E'_{\rm PBC} - E_{\rm PBC} \ , \tag{10}$$

i.e., the mass gap between the two R-sectors. From the fact that $\eta_{\rm V2}$ is finite in the flat phase and vanishes in the DOF and rough phases, it follows that this mass gap should be finite in the DOF phase and vanish in the flat phase. We will use both V2 and H2 to locate the preroughening phase boundary.

III. NUMERICAL RESULTS AND SUMMARY

The largest eigenvalues in each sector of the transfer matrix are obtained using the conventional iteration method. An arbitrary initial vector projects onto the largest eigenvector by applying the transfer matrix repeatedly. $E_{\rm PBC}$, $E_{\rm H1}$, and $E_{\rm H2}$ are easily found by this method. $E'_{\rm PBC}$ is obtained by choosing the initial vector in the $R=-1$ sector. The state vector is (2×3^N) dimensional for an semi-infinite strip of width N. The maximum strip width we can handle is $N=12$.

First, we focus on particular paths through the parameter space to illustrate the existence of the rough, DOF, and the flat phases. The FSS amplitude

$$S_{\rm H1}(N) \equiv \frac{\eta_{\rm H1} N}{2\zeta} \tag{11}$$

of the H1 type interface must converge to K_g in the rough phase (see Eq. (4)). Numerical data of $S_{\rm H1}(N)$ along the line $E_A = 0.1$ are presented in Fig. 5 (a). It shows that $\eta_{\rm H1}$ scales as $\frac{1}{N}$ with continuously-varying amplitudes at small E_B (high temperatures). The $\frac{1}{N}$ scaling breaks down at large E_B. This means that η_A or η_B becomes nonzero. The roughening transition should take place when $S_{\rm H1}(N)$ reaches the universal Kosterlitz-Thouless value $\frac{\pi}{2}$. This value is marked in Fig. 5 (a) by a dashed line, and indeed it crosses the numerical curve in the crossover region. So the numerical data in Fig. 5 (a) support that there is the rough phase at high temperatures, separated from the DOF or flat phase through a KT roughening transition.

We present also the FSS amplitudes of the interface free energy $\eta_{\rm H2}$ and the mass gap m, defined by

$$S_{\rm H2}(N) \equiv \frac{\eta_{\rm H2} N}{\zeta} \tag{12}$$

$$x(N) \equiv \frac{mN}{\zeta} \ , \tag{13}$$

along the line $E_B = 3.0$ in Figs. 5 (b) and (c). Both quantities show crossing points. They signal the crossover between two regions. One where η_A, the S_A-step free energy, vanishes (at small E_B) and one where it is finite (at large E_B). This confirms the existence of the DOF phase and the PR transition, since these free energy gaps must be finite in the flat phase but converge exponentially to zero in the DOF phase. For some reason, the convergence for V2 is dramatically better than for H2.

At KT type roughening transitions, the stiffness constant takes the universal value $\frac{\pi}{2}$. So we obtain a sequence of estimates of the roughening transition line by applying the condition $S_{\rm H1}(N) = \frac{\pi}{2}$ for each N. These are the roughening data points shown in Fig. 2. A sequence of estimates for the PR transition line between the flat and DOF phase can be obtained

from the crossing points of $x(N)$ and $x(N-2)$, and also those of $S_{\rm H2}(N)$ and $S_{\rm H2}(N-2)$. In Fig. 2 we show only the crossing points of V2 for $N = 6, 8, 10$ and 12. (Those of H2 are much less convergent, see Fig. 5 (b) and (c)).

The scaling theory of PR transitions, tells us that the critical fluctuations are described by the Gaussian model, but with K_g greater than the universal KT value $\frac{\pi}{2}$ of the roughening transition [11]. We investigate this scaling behavior by studying the FSS amplitudes of $\eta_{\rm H2}$ and m. In the Gaussian model, $S_{\rm H2}(N)$, does not vary continuously, instead it takes the universal value $\pi/4$ (see Eq. (5)). On the other hand, the V2 type mass gap should scale as [12]

$$m = \frac{\pi^2 \zeta}{2 K_g N} \ . \tag{14}$$

This is related to the fact that at $\Delta = 0$, the $R = -1$ and $R = +1$ sectors of $\mathbf{T}_{\rm PBC}$ are equivalent apart from a phase factor $e^{i\pi s_1}$ attached to all step variables s_1 at the seam (the first column of the lattice).

In Fig. 6 (a) we present the FSS amplitude of the mass gap m. The vertical axis is scaled as $\pi^2\zeta/(2mN)$, such that it represents K_g, see Eq. (14). K_g starts-off close to the universal value $\frac{\pi}{2}$ in the neighbourhood of the roughening transition, at $E_B \simeq 0.8$, and increases with E_B. This is in accordance with the assertion that the PR transition is described by the Gaussian model with continuously varying K_g greater than $\frac{\pi}{2}$. The FSS behaviour of $S_{\rm H2}$ along the PR line is shown in Fig. 6 (b). The dashed line denotes the universal value $\frac{\pi}{4}$ of the Gaussian model. The data at large E_B remain far from the universal value, though approach it. Like before, the convergence of this quantity is poor (see also Fig. 5(b)).

The PR transition line in Fig. 2 seems to penetrate into the rough phase. But this does not mean that there is another transition inside the rough phase. The rough phase is a critical phase where the mass gap scales as $O(1/N)$ on either side of the crossing points. The presence of crossing points of V2 inside the rough phase represents only a turn around in the corrections to scaling amplitudes for the amplitude.

The crossing of the two sets of lines in Fig. 2, the estimates for the roughening and PR

lines, confirms the existence of a multicritical point (E_{A_c}, E_{B_c}) where the PR and roughening transition merge. A sequence of estimates $(E_{A_c}(N), E_{B_C}(N))$ for the multicritical point is obtained by solving the two conditions $S_{\rm H1}(N) = \frac{\pi}{2}$ and $x(N) = x(N-2)$ simultaneously for each value of $N = 6, 8, 10$, and 12. These estimates are shown in Fig. 7. The arrows point towards power-law extrapolated values:

$$E_{A_c} = 0.41 \pm 0.03 \tag{15}$$

$$E_{B_c} = 0.89 \pm 0.01 \tag{16}$$

In summary, we have investigated the phase transitions in a model system for Si or Ge (001) type crystal surfaces with an uniaxial structure that switches direction at each mono-atomic step. We obtained the phase diagram from a numerical FSS study of the transfer matrix spectra. It consists of flat, rough, and DOF phases. The unusual topological properties of the surface stabilize the DOF phase in the absence of step-step interactions, which are crucial for the stabilization of the DOF phase in conventional surfaces. The location of the multicritical point where the PR transition line merges to the roughening transition line is determined numerically, $r_c \simeq 2.2$.

Specific crystals follow paths through Fig. 2 resembling straight lines as function of temperature, since the step energies are approximately constant. Our results shows that if the ratio $r = E_B/E_A$ is greater than a critical value $r_c \simeq 2.2$, the flat unreconstructed crystal undergoes a PR transition into the DOF phase followed by a roughening transition. In Si (001) surfaces, the ratio between the step energies is larger, $r \simeq 3$ [10]. We suggest therefore that Si (001) undergoes PR induced simultaneous deconstruction transition [7].

ACKNOWLEDGMENTS

We like to thank Prof. Doochul Kim for many helpful discussions and his hospitality during MdN's visit to the CTP at Seoul National University. This research is supported by NSF grant DMR-9700430, and by Korea Science and Engeneering Foundation through the Center for Theoretical Physics, Seoul National University.

REFERENCES

[1] R.J. Hamers, in *Scanning Tunneling Microscopy I*, edited by H.-J. Güntherodt and R. Wiesendanger (Springer-Verlag, Hong Kong, 1992); R. Becker and R. Wolkow, in *Scanning Tunneling Microscopy*, edited by J.A. Stroscio and W.J. Kaiser (Academic Press, New York, 1993).

[2] D.J. Chadi, Phys. Rev. Lett. **59**, 1691 (1987).

[3] D.E. Aspnes and J. Ihm, Phys. Rev. Lett. **57**, 3054 (1986).

[4] O.L. Alerhand, A.N. Berker, J.D. Joannopoulos, and D. Vanderbilt, Phys. Rev. Lett. **64**, 2406 (1990).

[5] E. Pehlke and J. Tersoff, Phys. Rev. Lett. **67**, 465 (1991).

[6] A.D. Johnson *et al.*, Phys. Rev. B **44**, 1134 (1991).

[7] M. den Nijs, J. Phys. A **30**, 397 (1997).

[8] M. den Nijs, J. Phys. A **18**, L549 (1985).

[9] K. Rommelse and M. den Nijs, Phys. Rev. Lett. **59**, 2578 (1987); M. den Nijs and K. Rommelse, Phys. Rev. B **40**, 4709 (1989).

[10] N.C. Bartelt, R.M. Tromp, and E.D. Willians, Phys. Rev. Lett. **73**, 1656 (1994); N.C. Bartelt and R.M. Tromp, Phys. Rev. B **54**, 11731 (1996).

[11] M. den Nijs, in *Phase Transitions in Surface Films*, edited by H. Taub *et al* (Plenum Press, New York, 1991).

[12] J.D. Noh, unpublished.

FIGURES

FIG. 1. Topology of S_A and S_B type step excitations on an unreconstructed Si (001) type surface.

FIG. 2. The phase diagram of the model defined in Eq. (1). The roughening transition lines are obtained from $S_{\rm H1} = \frac{\pi}{2}$ for $N = 6$ ($\Box$), 8 ($\circ$), and 10 ($\triangle$). Preroughening transition lines are obtained from the crossing points of $x(N)$ and $x(N-2)$ for $N = 6$ ($\Box$), 8 ($\circ$), 10 ($\triangle$), and 12 ($\bigtriangledown$). The lines between the data points are guides to the eyes.

FIG. 3. Step excitation type frustrations induced by the H1 (a), H2 (b), V1 (c), and V2 (d) boundary conditions. The uniaxial direction in each domain of flat region is shown to help identifying the steps.

FIG. 4. The transfer matrix set-up. The rows of a square lattice are rotated by 45°. The aspect ratio ζ between the lattice constants in the horizontal and vertical directions is equal to 2. Height and step variables are defined on faces and bonds of the lattice, respectively.

FIG. 5. Typical data of the FSS amplitude of the interface free energies $\eta_{\rm H1}$ (a), $\eta_{\rm H2}$ (b) and the mass gap m (c). Different symbols ($\Box$ for $N = 6$, $\circ$ for $N = 8$, $\triangle$ for $N = 10$, and $\bigtriangledown$ for $N = 12$) are used to distinguish the strip widths N. The lines are guides to the eyes.

FIG. 6. FSS amplitudes of m (a) and $\eta_{\rm H2}$ (b) along the preroughening transition line. Different symbols ($\Box$ for $N = 6$, $\circ$ for $N = 8$, $\triangle$ for $N = 10$, and $\bigtriangledown$ for $N = 12$) are used to distinguish the strip widths N.

FIG. 7. Estimates $(E_{A_c}(N), E_{B_c}(N))$ for the location of the multicritical point for $N = 6, 8, 10,$ and 12. The extrapolated values are marked by arrows.

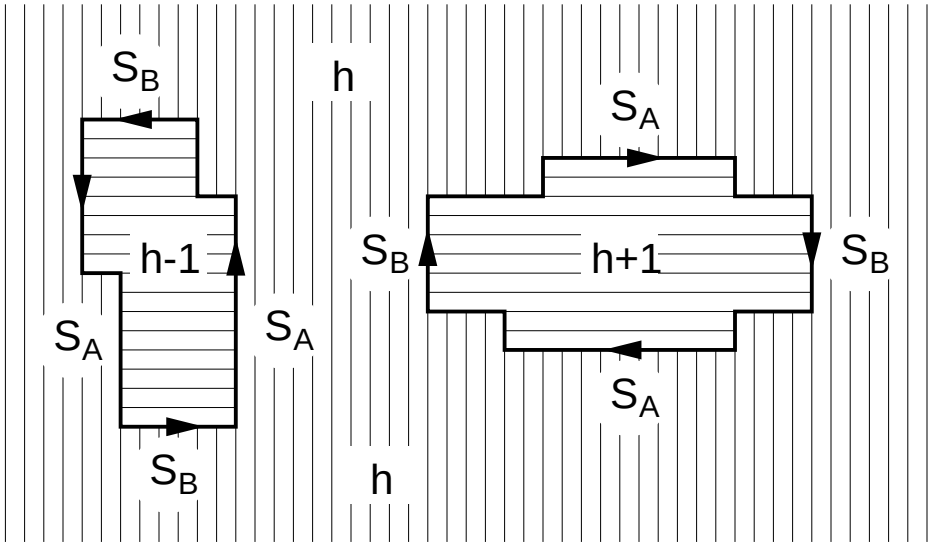

Figure 1 of Noh and den Nijs

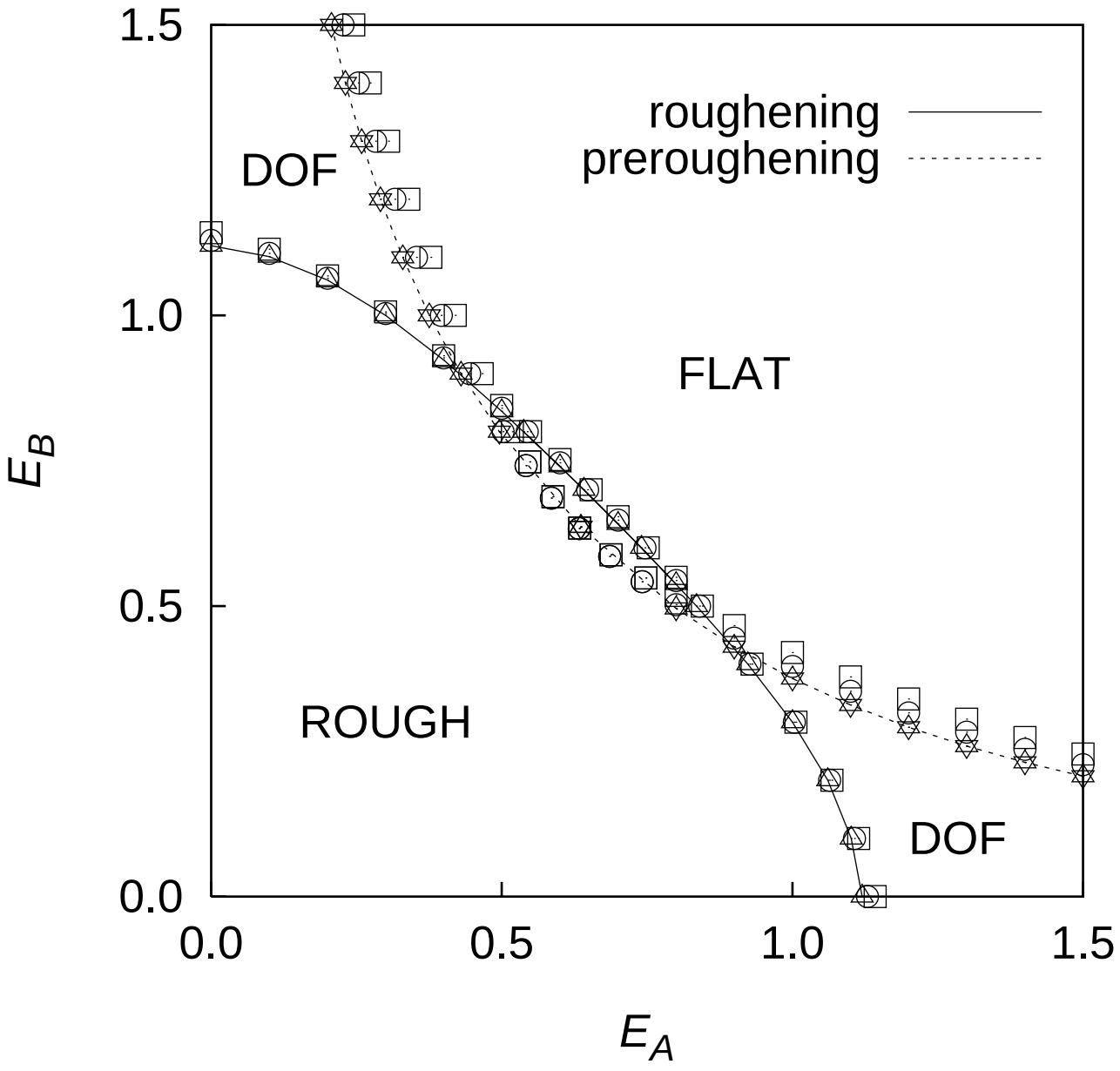

Figure 2 of Noh and den Nijs

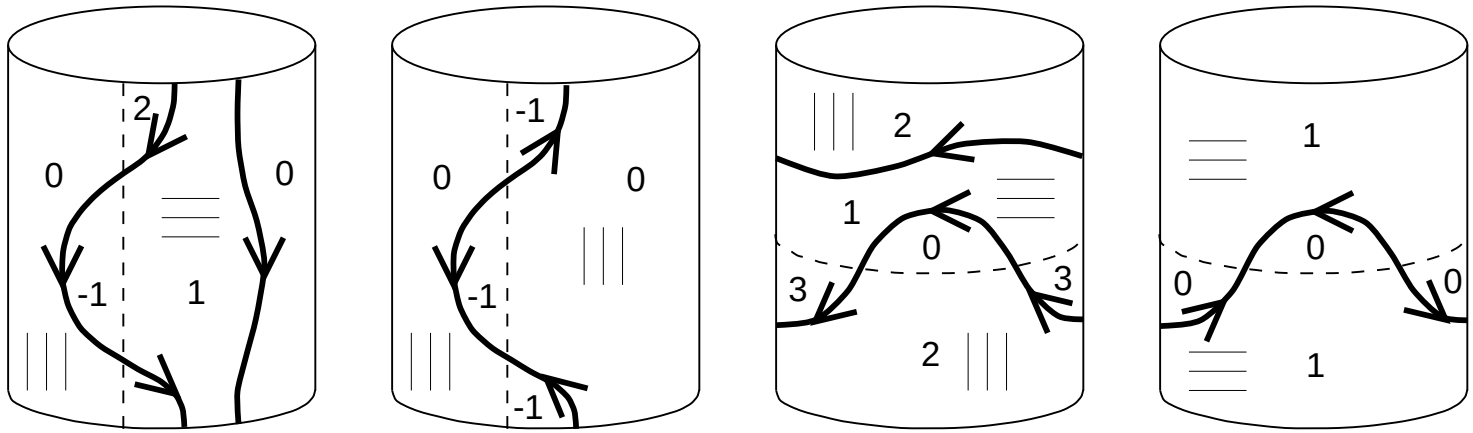

(a) (b) (c) (d)

Figure 3 of Noh and den Nijs

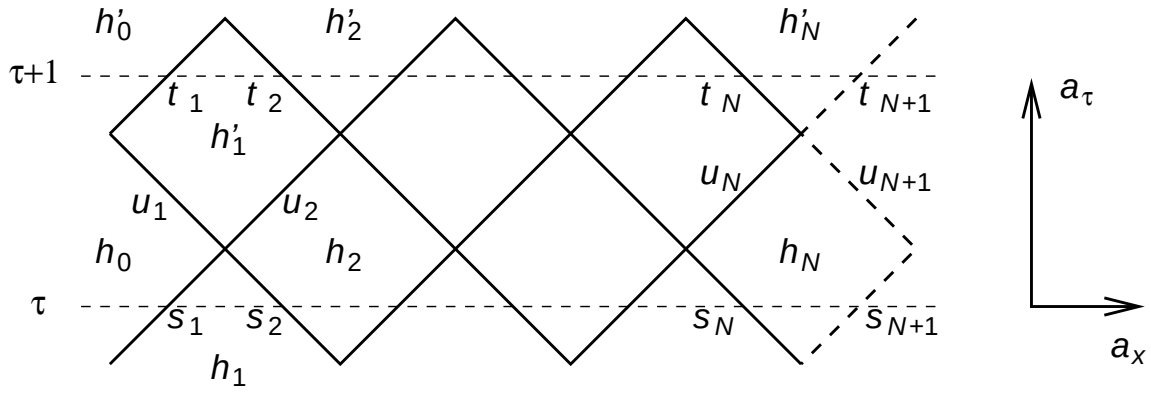

Figure 4 of Noh and den Nijs

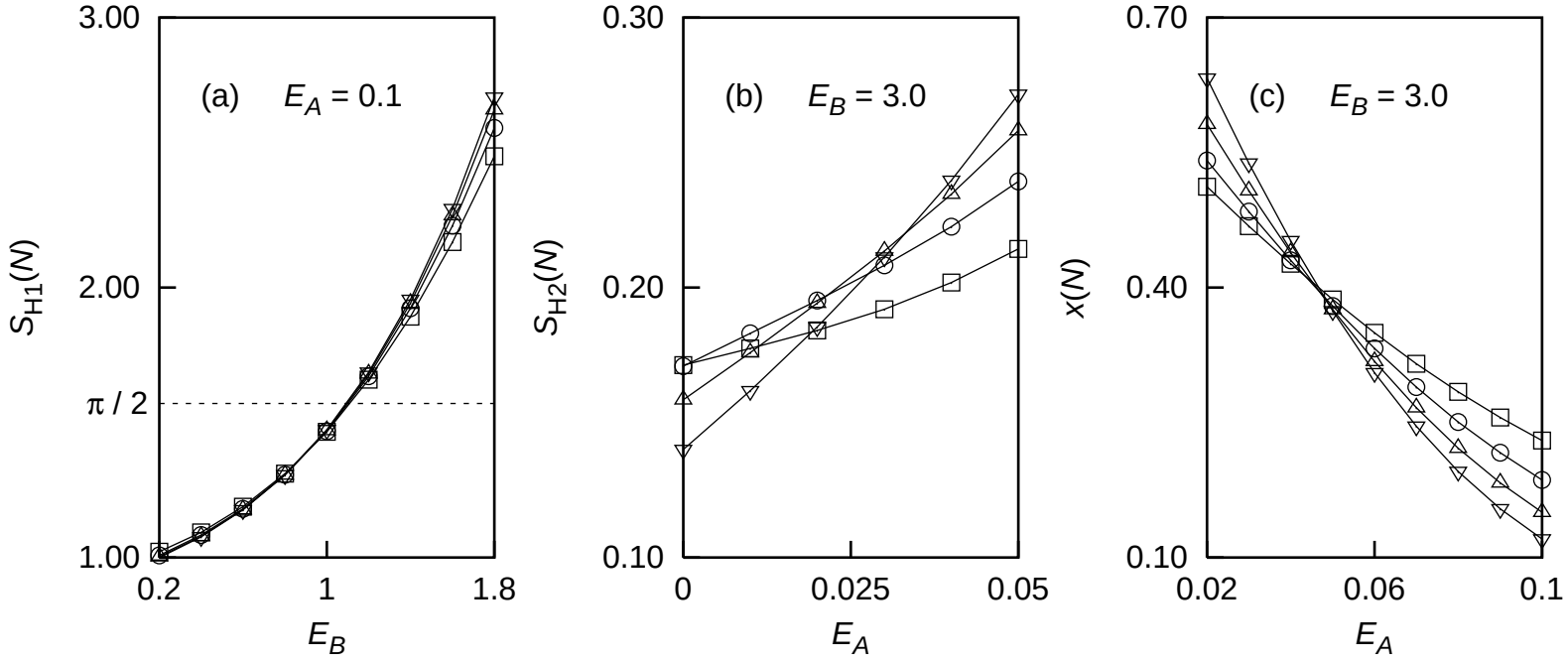

Figure 5 of Noh and den Nijs

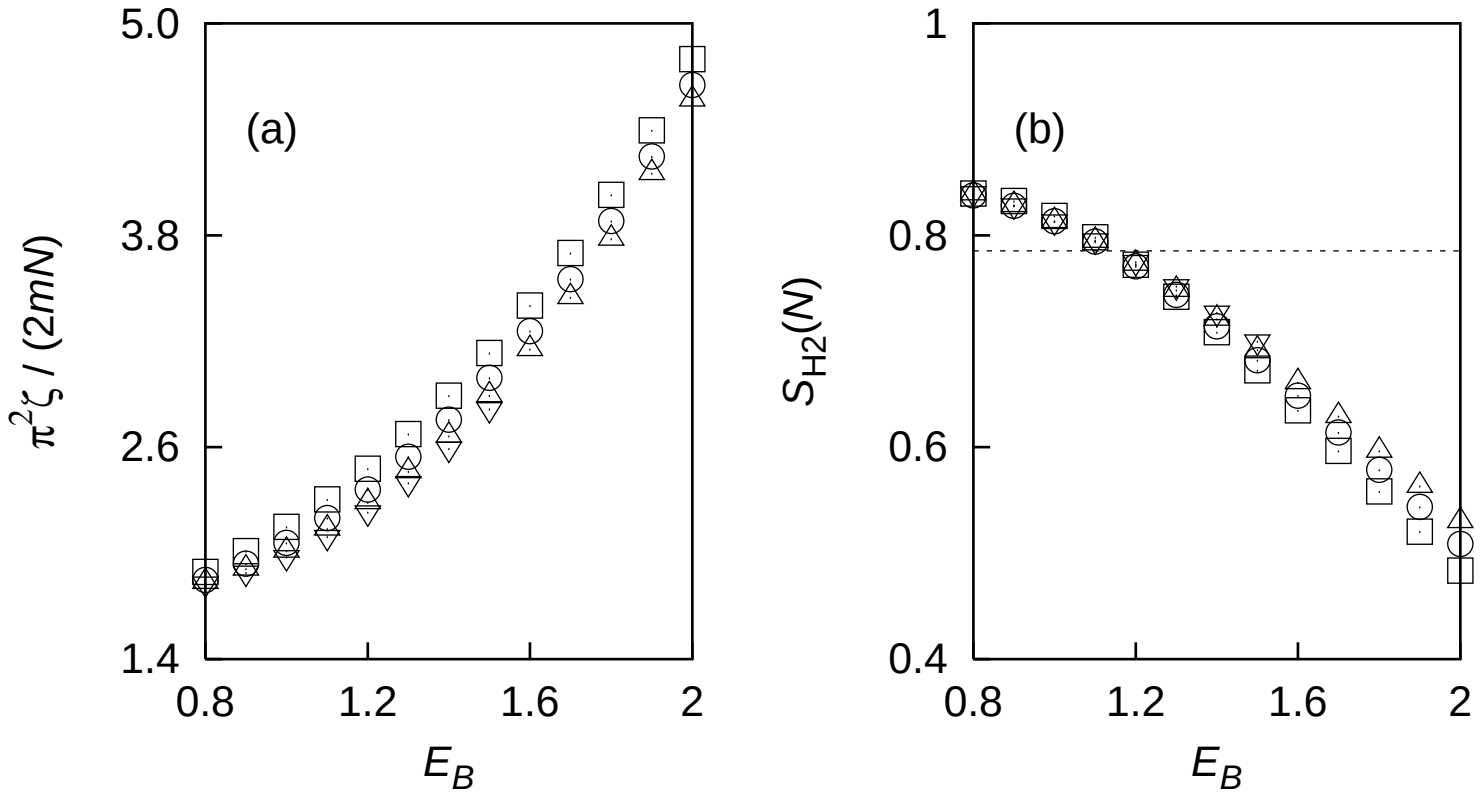

Figure 6 of Noh and den Nijs

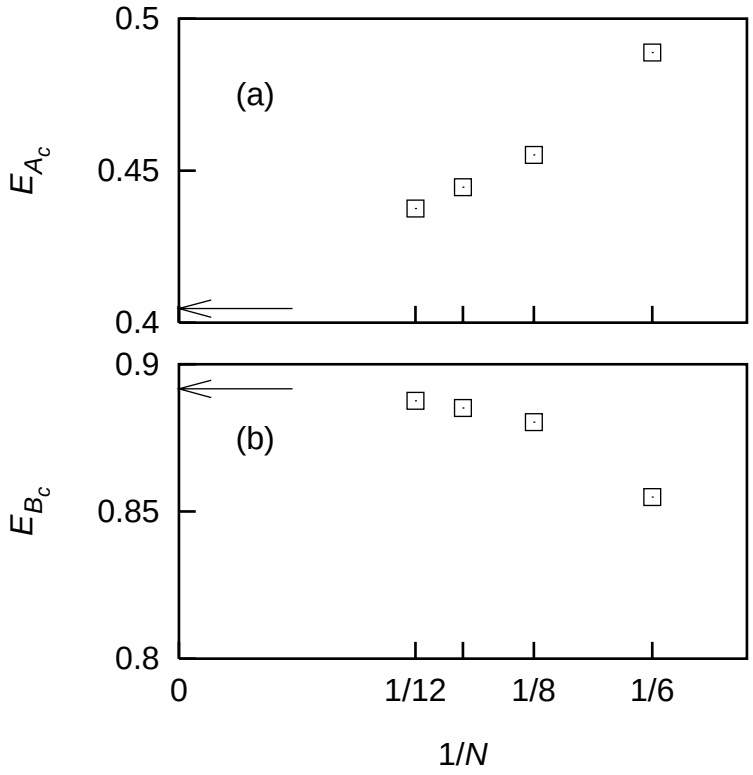

Figure 7 of Noh and den Nijs